Deep Neural Network Assisted Distributed Strain and Temperature Fiber Sensor System for Natural Gas Pipeline Monitoring

Nageswara Lalam, *Member, IEEE*, Hari Bhatta, Sandeep Reddy Bukka, Pengdi Zhang, Nathan Diemler, Alexander Shumski, Paul R. Ohodnicki, *Member, IEEE*, Michael P. Buric, and Ruishu F. Wright

***Abstract*— Natural gas pipeline integrity monitoring is crucial to detect potential leaks, find structural issues, and prevent environmental damage. This article presents a system of natural gas pipeline monitoring that uses a specialized double Brillouin peak sensing fiber along with the Brillouin optical time domain analysis (BOTDAs) technique. The calibrated sensing fiber coefficients for strain and temperature are 41.8 kHz/$\mu\varepsilon$ and 0.9 MHz/°C for peak 1; and 47.2 kHz/$\mu\varepsilon$, and 1.11 MHz/°C for peak 2, respectively. Initially, lab tests were performed by installing a short section of double Brillouin peak fiber (DBPF) on a 1-in steel pipe under pressure up to 1000 per square inch (psi) at elevated temperatures. Simultaneous distributed measurements of temperature and pressure-induced hoop strain were successfully measured. Considering the long processing speed to extract Brillouin frequency shift (BFS), we employ a novel probabilistic deep neural network (PDNN) framework for rapid BFS prediction. Additionally, using the Finite Element Method, the effects of the pipeline pressure on hoop strain were modeled and compared to the experimental hoop strain under the same set of pipeline conditions. Finally, an actual 4-in outer diameter steel natural gas pipeline was used for pilot-scale tests, where hoop strain was measured at various pressure levels. Leaks were simulated to demonstrate accurate pipeline integrity monitoring. At an internal pipe pressure of 1000 psi, hoop strain of approximately 300 $\mu\varepsilon$ was observed, and the sensitivity was calculated as 0.28 $\mu\varepsilon$/psi. The results of this pilot-scale study demonstrated that the system is capable of performing distributed monitoring sufficient to detect pipeline pressure and the presence of leaks to ensure the safe operation of gas pipelines in the field.**

Received 26 March 2024; revised 28 July 2024; accepted 4 October 2024. Date of publication 3 March 2025; date of current version 17 March 2025. This work was supported by the U.S. Department of Energy's (DOEs) Office of Fossil Energy and Carbon Management through the National Energy Technology Laboratory (NETL) Research and Innovation Center's Natural Gas Infrastructure Field Work Proposal under Grant 1022424. The Associate Editor coordinating the review process was Dr. Siliang Lu. *(Corresponding author: Nageswara Lalam.)*

Nageswara Lalam, Sandeep Reddy Bukka, Nathan Diemler, and Alexander Shumski are with the National Energy Technology Laboratory, Pittsburgh, PA 15236 USA, and also with the Leidos Research Support Team, Pittsburgh, PA 15236 USA (e-mail: nageswara.lalam@netl.doe.gov).

Hari Bhatta is with the National Energy Technology Laboratory, Pittsburgh, PA 15236 USA, and also with Oak Ridge Institute for Science and Education, Oak Ridge, TN 37830 USA.

Pengdi Zhang and Paul R. Ohodnicki are with the Department of Mechanical Engineering and Materials Science, University of Pittsburgh, Pittsburgh, PA 15213 USA.

Michael P. Buric is with the National Energy Technology Laboratory, Morgantown, WV 26505 USA.

Ruishu F. Wright is with the National Energy Technology Laboratory, Pittsburgh, PA 15236 USA.

Digital Object Identifier 10.1109/TIM.2025.3547114

***Index Terms*— Deep neural network (DNN), distributed sensing, pipeline monitoring, strain and temperature sensing.**

I. Introduction

THE natural gas pipeline network is a critical component of the nation's energy infrastructure that enables reliable and efficient transportation of natural gas to support a wide range of industries and consumers across the country. The U.S. natural gas pipeline network is one of the largest and most comprehensive in the world. It is comprised of over three million miles of pipelines, ranging from large interstate transmission pipelines to smaller intrastate and distribution pipelines. The system is categorized into gathering, transmission, and distribution networks. Across the network, maximum pressures can range from several hundred to several thousand pounds per square inch (psi). Gathering pipelines collect natural gas from production wells and transport it to processing plants or larger transmission pipelines [1]. Transmission pipelines are responsible for moving natural gas across long distances, often spanning multiple states. These high-pressure pipelines are designed to transport large volumes of gas from production areas to distribution hubs, storage facilities, or local distribution companies. Lastly, distribution pipelines deliver natural gas directly to homes, businesses, and other end users, typically operating at lower pressures [2]. The U.S. natural gas pipeline network is subject to stringent regulatory oversight at both the federal and state levels. Regulatory agencies, including the Federal Energy Regulatory Commission (FERC), the Pipeline and Hazardous Materials Safety Administration (PHMSA), state public utility commissions, and the Environmental Protection Agency (EPA) all work to ensure the safe and efficient operation of the pipeline network.

Monitoring the natural gas pipeline network is essential for ensuring safe, reliable, and efficient transportation of natural gas from production areas to consumption centers. Various regulatory requirements, industry standards, and best practices govern the monitoring of natural gas pipelines in the United States [3]. The primary goal of gas pipeline integrity monitoring is to identify potential leaks, thinning, and other hazardous conditions that can lead to structural damage or environmental pollution. By implementing effective monitoring practices, pipeline operators can identify and address potential issues before they escalate into major problems [4].

© 2025 The Authors. This work is licensed under a Creative Commons Attribution 4.0 License.
For more information, see https://creativecommons.org/licenses/by/4.0/

Some common methodologies exist for pipeline monitoring today. Hoop strain, also known as circumferential stress, represents the stress experienced by the pipe's wall in the circumferential direction (perpendicular to both the pipe axis and radius) due to internal pressure and external loads. The current practice of monitoring hoop strain often involves using individual electrical single-point strain gauges which are commonly mounted on pipe surfaces. Another common method for assessing hoop strain is ultrasonic testing, which is a non-destructive method relying on sound-wave propagation using portable measurement tools. In addition to these monitoring methods, periodic visual inspections and in-line inspection (ILI) using smart pigs equipped with sensors are conducted to identify any anomalies such as corrosion, dents, or external stresses [5], [6]. To ensure high levels of safety and prevent catastrophic failures, it is challenging to monitor longer lengths of pipelines in real time using the present monitoring technologies, which involve either point-based sensors or periodic inspections. In addition, data transmission to monitoring stations and connectivity can be difficult, which results in delays in detecting and responding to critical events.

Distributed optical fiber sensor (DOFS) systems offer a promising solution for continuous and distributed monitoring, enabling precise measurements of physical parameters over long distances. DOFS strain measurements can be translated into hoop strain and correlated to pipeline pressure. Unlike traditional point sensors, which provide measurements at specific locations, DOFS can provide spatially resolved continuously monitored real-time data over hundreds of kilometers. Distributed real-time monitoring of leakage rates, pressure, temperature, and strain variations is made possible by DOFS technology [7], [8]. Among the various types of DOFS systems, Brillouin optical time domain analysis (BOTDAs) sensor systems have demonstrated utility in long-distance distributed temperature and/or strain sensing. In BOTDA, a pump laser is modulated into short pulses and injected into one end of an optical fiber, while a counter-propagating continuous-wave probe wave is injected from the opposite end of the fiber. The interaction between the pump and probe waves in the fiber generates stimulated Brillouin scattering. As the pump pulses travel along the fiber, they generate localized Brillouin scattering when the pulse is present at a given location. The backscattered signal interacts with the counter-propagating probe wave, creating stimulated Brillouin scattering, the detected beat frequency known as Brillouin frequency shift (BFS), which lies between 10 and 11 GHz in fused silica optical fiber. The BFS depends on the physical properties of the sensing fiber including material composition of the fiber core. By analyzing the time delay between the pump pulse and the collected backscattering signal, the BOTDA system can determine the location of any scattering event along the fiber. This time-domain information, combined with the frequency shift data, provides a distributed profile of temperature and strain. Typically, in BOTDA, the BFS is obtained by fitting the local Brillouin gain spectrum (BGS) at each point to a second-order polynomial function. In practical applications, temperature and strain can simultaneously affect the BFS; leading to cross-sensitivity.

A few research groups have demonstrated the use of the DOFS system for pipeline monitoring in the literature. In 2018, Feng et al. [9] proposed a pipeline monitoring scheme for distributed strain and temperature by installing two types of optical fibers, one for strain and the other for temperature. A Raman-based distributed temperature sensor system was selected to perform the temperature measurement, while the BOTDA system was used for strain measurements, which enabled simultaneous sensing of strain and temperature. However, this method is complicated and requires two optical fibers to be installed, as well as requiring two expensive optical interrogators to provide both strain and temperature data. Recently, Bertulessi et al. [10] demonstrated the ability to detect strain associated with pressure anomalies along a water pipeline and demonstrated measurements of pipeline hoop strain by wrapping the optical fiber around the pipeline circumference. Zhang et al. [11], constructed a 4 m long polyvinyl chloride (PVC) pipeline in the lab and monitored pipeline deformation by applying different levels of load on the pipe. These prior attempts emphasize that the cross-sensitivity between strain and temperature is a major challenge in BOTDA systems and that no straightforward solution to measuring both parameters in pipelines has been demonstrated.

In addition to the issues encountered by other groups with measurand cross-sensitivity, the problem of precisely determining the peak of the BGS is significant and time-consuming for long fibers producing large datasets. In order to handle the massive amounts of data from the BOTDA faster, and to more precisely extract temperature and strain information, novel signal processing techniques are needed. For example, the local BFS along the sensing fiber length is commonly extracted by using nonlinear curve fitting models such as follows: 1) Lorentzian; 2) Gaussian; 3) pseudo-Voigt; and 4) quadratic curve fitting [12]. Measurement accuracy using these fitting models may be inadequate in real-world scenarios because of significant noise in the BGS, particularly for longer (multi-kilometer) lengths. Furthermore, as conventional fitting algorithms frequently need multiple iterations to reach convergence, the processing time of these fitting models presents a challenge for long-range real-time sensing. Therefore, a growing focus is on developing improved signal processing algorithms that manage noisy BGS data rapidly by utilizing state-of-the-art machine learning techniques like deep neural networks (DNNs) [13]. In 2022 Qi et al. [14], demonstrated a convolutional neural network (CNN) algorithm to accelerate the data processing speed for a polarization-insensitive BOTDA system. Using a 900-m long sensing fiber, the BFS extraction time was 1.91 s, which was about 13 times faster than conventional Lorentzian curve fitting. In 2019, Wang et al. [15] demonstrated a DNN BOTDA data processing system and compared it with the conventional equation-solving technique. The processing speed achieved for a 24 km long LEAF sensing fiber was 1.6 s and the strain/temperature uncertainties were 66 $\mu\varepsilon$/2.4 °C. Zheng et al. [16] experimentally demonstrated a DNN algorithm for a BOTDA system with a 10 km long standard single-mode fiber, which took 0.04 s for data processing. Wang et al. [17] proposed a denoising autoencoder combined with DNN based data processing for

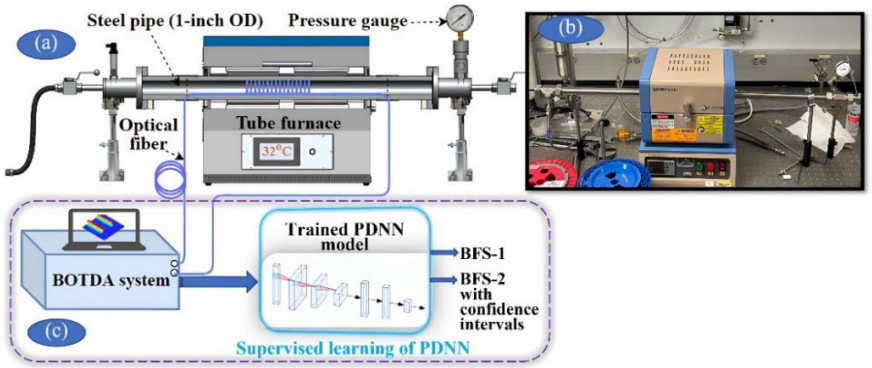

Fig. 1. (a) Schematic illustration of hoop strain and temperature measurement of pressurized steel pipe with circumferentially wrapped fiber. (b) Picture of the laboratory test setup. and (c) BOTDA system with PDNN-based data processing.

rapid temperature extraction. At the end of ~20 km sensing fiber, the temperature standard deviation was found to be 3.08 °C. However, the existing CNN/DNN models do not report the confidence intervals of the predicted parameters, and it is possible to further improve data processing speed while also reducing measurement uncertainties.

To the best of our knowledge, this study presents the first simultaneous measurement of pipeline temperature and hoop strain in both lab-scale and field experiments. This method requires only a single sensing fiber, and a single optical interrogation system for reporting both parameters in a single measurement. Additionally, we developed a probabilistic DNN (PDNN) for accurate BFS extraction from double Brillouin peak fiber (DBPF) with rapid processing speed while adding a new capability of providing confidence intervals with predicted mean. To further support experimental data, FEA simulations were conducted using Ansys software which were then compared to field scenarios. This permitted an accurate correlation of hoop strain to pipeline pressure.

The optical fiber that permits simplified discrimination between strain and temperature in this report is specially designed to produce two Brillouin peaks, each of which exhibits different strain and temperature coefficients. In the past, a number of different fibers have been demonstrated for discriminative strain and temperature measurements based on multiple Brillouin peaks, such as non-zero dispersion-shifted fiber, dual-core fiber, and photonic crystal fiber. However, the low gain exhibited by the second Brillouin peak led to increased measurement errors. The novel DBPF used here was designed with an enhanced second Brillouin peak gain by modifying the higher-order acoustic modes. Gain levels for both peaks exhibited by this fiber are similar in magnitude. Further information regarding the design and simulation of DBPF fibers can be found in [18] and [19].

II. Lab-Scale Pipeline Temperature and Hoop Strain Measurements

For the lab-scale experiments, we used a 40-in long steel pipe with an outside diameter of 1 in for measuring hoop strains and temperature changes simultaneously at various conditions. A 2.5 m DBPF test segment toward the end of the 180 m fiber spool was wrapped circumferentially and fixed with a strong adhesive glue at the center of the pipe as shown in Fig. 1(a). One end of the pipe was fit with a high pressure gas supply while the other end was connected to a pressure gauge and outlet valve. A mass-flow controller (Brooks 0254). The system was filled with nitrogen from a high-pressure cylinder (1000 psi) at flow rates upto 1500 sccm, and the vessel pressure was verified by an analog pressure gauge. Heating was applied to the system for temperature tests using an MTI OTF-1200X tube furnace for heating above ambient temperature. Common pipeline operating temperatures (<100 °C) could be applied. The overall schematic of the experimental setup and PDNN-based data processing is illustrated in Fig. 1. A photograph of the lab setup is shown in Fig. 1(b). Complete details of the BOTDA experimental setup and its data collection procedures can be found in our recent work [19].

Initially, we demonstrated pipeline pressure-induced hoop strain measurements. Thereafter, simultaneous measurements of hoop strain and temperatures were performed. The experimental setup was equipped with a controllable tube furnace and a gas pressure controller, thus allowing us precise control over both physical parameters. First, we emphasized measuring hoop strain while maintaining a steady temperature. We acquired relevant data at the ambient state (without applying pressure to the pipe and ambient room temperature of 22 °C) as our baseline. The pipe pressure was gradually increased with nitrogen gas to the desired pressure while performing measurements. The BOTDA system's pump pulsewidth was set at 20 ns, which corresponds to a spatial resolution of 2 m. In Fig. 2(a), the 3-D spectrum was acquired by scanning the Brillouin frequencies from 9.75 to 10.6 GHz with a step of 2 MHz. From Fig. 2, we can see that the gain levels of both peaks 1 and 2 are almost identical and are separated by >500 MHz. In order to discriminate between temperature, and strain, a 100 MHz frequency separation of the peaks is sufficient because both peaks will move to higher frequencies when strain, or temperature increases. Fig. 2(b) illustrates how the BGS shifts at various temperatures. We can see that the two peaks are well-separated, which will result in lower measurement error, uncertainty, and cross-sensitivity.

After baseline measurements, the pipe pressure was increased up to 1000 psi at 200 psi intervals. At each pressure level, the measurements were carried out and the BFS distribution was retrieved for the entire fiber length. The relative

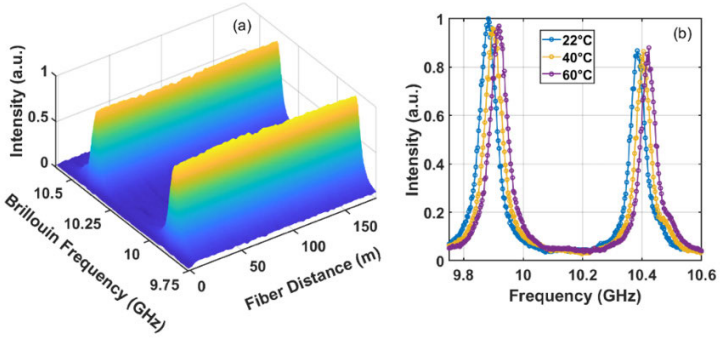

Fig. 2. (a) DBPF gain spectrum as a function of frequency and distance measured at pressure-free and ambient room temperature. (b) Extracted Brillouin gain spectra under different temperatures at the fiber end.

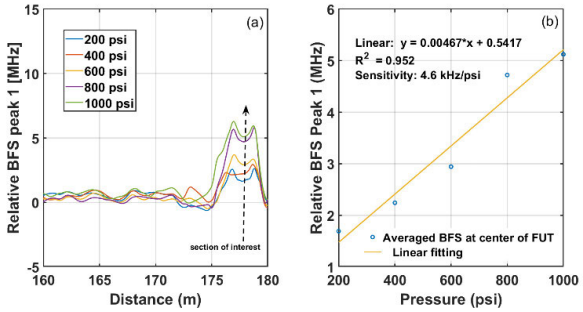

Fig. 3. (a) Relative BFS distribution of peak 1 as the pipeline pressure changes. (b) Resulting sensitivity of peak 1 BFS shift versus pipeline pressure.

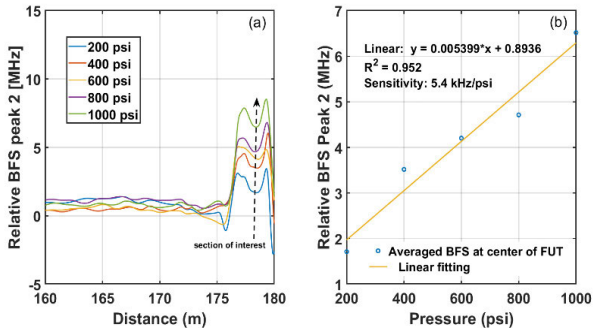

Fig. 4. (a) Relative BFS distribution of peak 2 as the pipeline pressure changes. (b) Resulting sensitivity of peak 2 BFS shift versus pipeline pressure.

BFS distribution of both Brillouin peaks versus fiber length is shown in Figs. 3(a) and 4(a) for different pressure levels applied. Figs. 3(b) and 4(b) plot the BFS versus pressure for both peaks, along with a linear interpolation of the data. The sensitivity is found using the slope of the linear curve fit in each figure. The sensitivity of the BFS to pressure changes was found to be 4.6 kHz/psi for peak 1 and 5.4 kHz/psi for peak 2. The BFS was measured over a central 1 m fiber under test (FUT) section was installed on the test pipe, which comprised 50 samples, and the average relative BFS versus applied pressure was calculated. The calculated sensitivity for peaks 1 and 2 is shown in Figs. 3(b) and 4(b), respectively. For peak 1, a 200 psi change in pressure results in a 22.1 $\mu\varepsilon$ change in hoop strain. Similarly, for peak 2, hoop strain changes of 22.5 $\mu\varepsilon$ were observed, and the difference in hoop strain results using peaks 1 and 2 is <0.5 $\mu\varepsilon$. It was observed that a change of 1000 psi resulted in a hoop strain of around 110 $\mu\varepsilon$ as expected. The strain sensitivity coefficients used were 41.8 kHz/$\mu\varepsilon$ for peak 1, and 47.2 kHz/$\mu\varepsilon$ for peak 2, along with temperature coefficients of 0.91 MHz/°C, and 1.11 MHz/°C for peaks 1 and 2, respectively [19].

Utilizing both peaks of the DBPF, where each peak has a different sensitivity coefficient for strain and temperature, simultaneous changes in temperature and strain can be evaluated independently. The relationship between the change in BFSs for peaks 1 ($\Delta\upsilon_{B1}$) and peak 2 ($\Delta\upsilon_{B2}$) and the change in temperature (ΔT) and strain ($\Delta\varepsilon$) are as follows [18], [19]:

$$\begin{bmatrix} \Delta\upsilon_{B1} \\ \Delta\upsilon_{B2} \end{bmatrix} = \begin{bmatrix} \mathrm{C}_{T1} & \mathrm{C}_{\varepsilon1} \\ \mathrm{C}_{T2} & \mathrm{C}_{\varepsilon2} \end{bmatrix} \begin{bmatrix} \Delta T \\ \Delta\varepsilon \end{bmatrix} \tag{1}$$

where C_{T1}, and C_{T2} are the temperature sensitivity coefficients, $\mathrm{C}_{\varepsilon1}$, and $\mathrm{C}_{\varepsilon2}$ are strain sensitivity coefficients for peaks 1 and 2, respectively. The temperature and strain are determined by solving (1) as follows:

$$\Delta T = \frac{\mathrm{C}_{\varepsilon2}.\Delta\upsilon_{B1} - \mathrm{C}_{\varepsilon1}.\Delta\upsilon_{B2}}{\mathrm{C}_{T1}.\mathrm{C}_{\varepsilon2} - \mathrm{C}_{T2}.\mathrm{C}_{\varepsilon1}} \tag{2}$$

$$\Delta\varepsilon = \frac{\mathrm{C}_{T2}.\Delta\upsilon_{B1} - \mathrm{C}_{T1}.\Delta\upsilon_{B2}}{\mathrm{C}_{T2}.\mathrm{C}_{\varepsilon1} - \mathrm{C}_{T1}.\mathrm{C}_{\varepsilon2}}. \tag{3}$$

For the discriminatory measurements of strain and temperature, the baseline data was measured under ambient conditions. Thereafter, the pressure changed from ambient to 400 psi and finally to 800 psi. At a fixed pressure of 800 psi, we raised the temperature to 45 °C using a tube furnace. Employing established equations for temperature and strain evaluations [19], and utilizing both retrieved BFS peaks as shown in Fig. 5, we derived simultaneously measured results that closely matched the expected values, as shown in Fig. 6. Notably, the strain obtained at 800 psi was approximately 110 $\mu\varepsilon$, which lies within the margin of <20 $\mu\varepsilon$ error. Some increased hoop strain (125 $\mu\varepsilon$) was observed when the temperature was changed to 45 °C, which could be due to the actual nitrogen pressure being >800 psi when the temperature is 45 °C. This is logical for the ideal gas such as nitrogen. Also, temperature measurement at 45 °C shows an average accuracy error of approximately $\sim$1 °C. We see that the central section of the FUT exhibited the capability to independently follow changes in both temperature and strain, in alignment with discriminatory measurement capabilities of DBPF, and

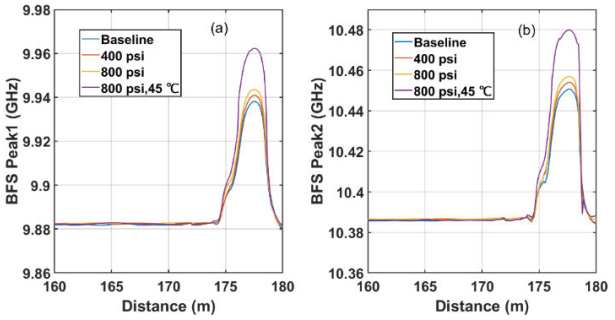

Fig. 5. Measured BFS distribution of (a) peak 1 and (b) peak 2, for the discriminatory measurements at different conditions of pressure and temperature.

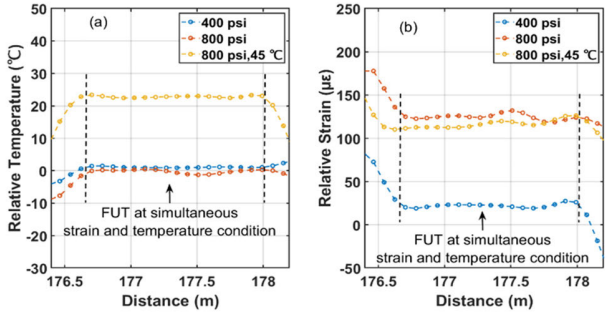

Fig. 6. (a) Relative temperature distribution. (b) Pressure-induced hoop strain changes calculated by (1) and (2).

it is possible that we might see better results when keeping the experiment under perfectly controlled temperature/pressure conditions.

A. PDNN Based Data Processing

Conventionally, the BFS is computed from the measured raw BGS spectrums over the fiber length by using nonlinear least square fitting methods, such as Lorentzian, quadratic, and pseudo-Voigt fitting models [12]. However, the processing time required by traditional curve fitting models is extensive with large measurement uncertainties, which makes real-time sensing unachievable. After verifying the discriminatory capabilities of the DBPF, we attempted to accelerate the processing time by developing a PDNN framework for rapid BFS estimation along with a confidence interval [20], [21]. However, this initial model was only tested on standard single-mode fibers, which feature a singular BGS peak. This approach required further refinement to accurately address specialty fibers that exhibit double BGS peaks, which we used in this study. Later, the original PDNN framework was improved and adapted to enable the concurrent estimation of multiple BFSs.

A comprehensive diagram detailing this advanced framework and its training methodology can be found in Fig. 7. The PDNN was trained using a simulated dataset generated based on the following Lorentzian equation [7]:

$$g(\nu;\nu_{B1},w_1,w_2,\nu_{B2}) = \frac{w_1^2}{4(\nu-\nu_{B1})^2+w_1^2} + g_0\frac{w_2^2}{4(\nu-\nu_{B2})^2+w_2^2} \quad (4)$$

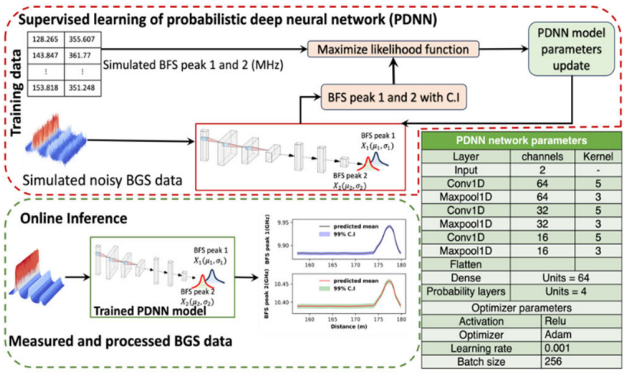

Fig. 7. Schematic of proposed PDNN to predict the BFSs with confidence intervals.

where ν_{B1}, ν_{B2} are the BFSs, and w_1, w_2 are the full width at half maximum (FWHM) for peaks 1 and 2, respectively. g_0 is the normalized Brillouin gain amplitude. In total, 50 000 BGS samples were generated by varying the above parameters. All the parameters were sampled from uniform probability distributions, $y \sim \mathbb{U}(y_l, y_u)$, $p(y) = (1/(y_u - y_l)), \forall y_l \le y \le y_u$ between lower and upper bounds including noise amplitude, s, and is given as follows.

1) $\nu_{B1}, \nu_{B2} \sim \mathbb{U}(165, 257), \mathbb{U}(664, 770)$.
2) $w_1, w_2 \sim \mathbb{U}(40, 110), \mathbb{U}(35, 120)$.
3) $g_0 \sim \mathbb{U}(0.7, 0.99)$.
4) $s \sim \mathbb{U}((1/100), (1/5))$.

The BGS spectra with broad frequencies allow the PDNN to accurately predict system behaviors under diverse operational conditions and adapt to different fiber types of sensing fibers with distinct BFSs. The ranges for the FWHM values, which were carefully designed to capture the variability in BGS linewidth due to factors such as fiber doping levels or temperature fluctuations. Training over a wide range of possible values ensures robust PDNN. Robust training also allows the PDNN to handle different levels of spectral broadening, a crucial feature for optical sensing and signal processing applications. The noise scale parameters were selected based on typical operational variations and experimental conditions. By integrating these realistic and varied parameter ranges, the training setup is optimized to enhance the model's generalization capabilities and ensure its applicability to practical environments. These ranges ensure that the PDNN can effectively manage signal intensity and noise variations, which are critical for optimizing output and maintaining robust performance in real-world scenarios.

Fig. 8 demonstrates the comparison between PDNN predictions and the traditional nonlinear least squares fitting method at 1000 psi pressure. The data processing speed was greatly reduced to ~0.38 s based on PDNN, while conventional curve fitting took ~3.79 s to process the same BGS data. It is apparent that the data processing time was reduced greatly while maintaining the minimum standard deviations (σ). The PDNN model was optimized to leverage its architectural efficiencies and realize the real-time monitoring capability with minimal BFS estimation errors. The primary advantage of employing PDNN lies in its computational efficiency, achieving an

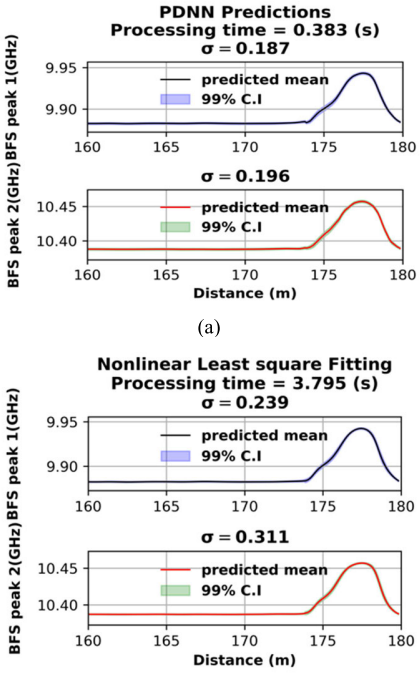

Fig. 8. (a) PDNN predictions with C. I. (b) Standard curve fitting with C. I for BGS data obtained at 1000 psi pipe pressure.

approximately tenfold increase in speed compared to the conventional Lorentzian fitting technique. This improvement in processing time becomes particularly significant when analyzing data from hundreds of kilometers of fiber. Importantly, the computational acceleration does not detract from the accuracy of PDNN's predictions. We observe, that the confidence intervals generated by PDNN are similar to those obtained through curve-fitting methods. Fig. 9 presents the PDNN forecasts of relative BFSs for peaks 1 and 2 across various pressures, alongside comparisons to the curve fitting approach. The PDNN model consistently replicates the expected behavior, where an increase in pressure corresponds to a higher BFS peak shift. The development and refinement of the PDNN framework will proceed, supported by further validations using data collected by our research. It is clearly observed that PDNN-based extraction of BFSs agrees well with conventional methods. As we can see in Fig. 9, the maximum difference in estimations between the two methods at the same section of the FUT under the same local environmental condition is within the 1 MHz range. An error margin within the 1 MHz range (which corresponds to the $\sim$20 $\mu\varepsilon$ or $\sim$1 °C) is generally expected for uncertainties in BOTDA measurements. It is obvious that by increasing the average, we might be able to reduce noises in the gain traces and thus could enhance the BFS accuracy of the measurements.

B. Simulation Analysis of Pipeline Hoop Strain

A finite element analysis of a pressurized pipeline was also performed using Ansys software. Results were compared with the experimental hoop strain results obtained in the laboratory environment. The pipeline material properties, including

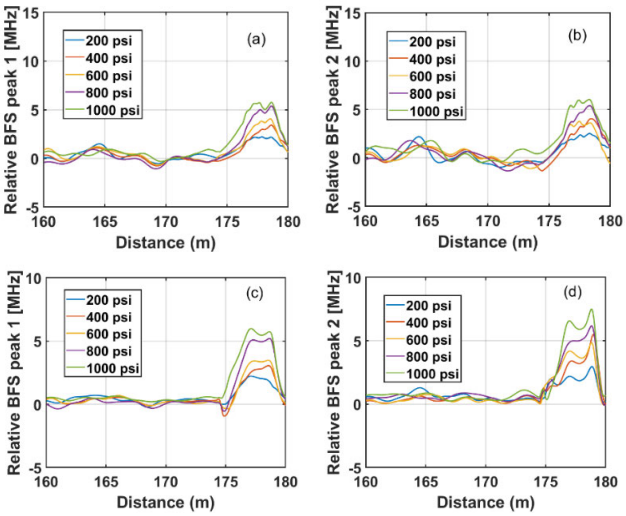

Fig. 9. PDNN predictions of relative BFSs. (a) and (b) Peaks 1 and 2. Standard curve fitting method of relative BFSs. (c) and (d) Peaks 1 and 2 at various pressure levels.

TABLE I
PARAMETERS USED TO MODEL THE STEEL PIPELINE

Steel Pipeline Parameter	Value
Length (inch)	40
Outside Diameter (inch)	1
Wall thickness (inch)	0.0415
Density ($\frac{kg}{m^3}$)	7,850
Young's Modulus (Pa)	$21{\times}10^{10}$
Poisson Ratio	0.32

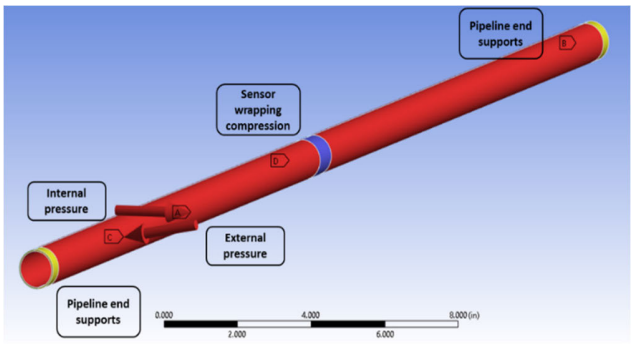

Fig. 10. Complex boundary and loading conditions for pipeline simulation.

Young's modulus, Poisson's ratio, and yield strength, as well as the dimensional properties, including wall thickness, length, and diameter, are shown in Table I.

This simulation analysis compares the results of the simulated hoop strain with experimental data to validate the simulation model and better understand the pipeline hoop strain behavior under various conditions. Also, the model's realistic boundary conditions were applied to the model, including fixed supports, pressure loads, and correct sensor position as illustrated in Fig. 10.

The simplistic model in our simulation setup is a first approximation, and then more complex boundary and loading

conditions are considered for a full simulation. As illustrated in Fig. 10, the pipeline's endpoints are rigidly anchored, and the sensor fiber is circumferentially mounted on the pipeline's outer surface at the midpoint to replicate the experimental conditions [shown in Fig. 1(a)]. With this configuration, variances in the pipeline deformation under various internal pressures translated into hoop strain variations. Labels "A" and "C" in Fig. 10 represent the pipeline's internal and exterior pressures, respectively. The pipe support stands and the fiber sensor location are labeled as "B" and "D," respectively.

The simulation considers the effects of isotropic or orthotropic material on curvature variation, and the pipe is commonly represented as a thin-walled circular cylinder. The key parameter in these simulations is the circumferential or hoop strain, which is a measure of pipe deformation in the circumferential direction due to internal pressure [22]. The simulation considers various factors that affect the stress and strain distribution over time. The goal is to accurately predict how the structure responds to internal pressures, considering both the material properties and the loading conditions. This strain is directly related to the internal pressure through the following equation [23]:

$$\sigma_t = P\left(\frac{r_e}{r}\right)^2\left(\frac{1}{\left(\frac{r_e}{r_i}\right)^2 - 1}\right) \tag{5}$$

where σ_t is the tangential stress, P is the internal pressure, r is the radius at the point of interest, r_e is the outer radius, and r_i is the inner radius. The circumferential or hoop strain, ε_{h} can be calculated using Hooke's Law in the elastic region

$$\varepsilon_{\mathrm{h}} = \frac{\sigma_t}{E}; \quad \Delta\varepsilon_{\mathrm{h}} = \frac{\varepsilon_{\mathrm{h,final}} - \varepsilon_{\mathrm{h,initial}}}{\varepsilon_{\mathrm{h,initial}}} \tag{6}$$

where E is the modulus of elasticity of the steel, $\Delta\varepsilon_{\mathrm{h}}$ is the relative change in hoop strain, $\varepsilon_{\mathrm{h,final}}$ is the final hoop strain, and $\varepsilon_{\mathrm{h,initial}}$ is the initial hoop strain. The simulation process involves applying different internal pressures P and calculating the resulting circumferential strain, ε_{h}. Fig. 11(b) represents the change in circumferential strain concerning the change in internal pressure. Fig. 11(a) shows the measured experimental hoop strain was approximately 83 $\mu\varepsilon$ at 1000 psi pressure, which is close to the simulated value of 87 $\mu\varepsilon$ at 1000 psi as shown in Fig. 11(b). This verifies the accuracy of the sensor system in performing pressure estimations using hoop strain.

III. Pilot-Scale Testing of the Sensor System for High-Pressure Natural Gas Pipelines

To verify sensor system operation, field tests were performed using larger pipeline systems with leak-simulation capabilities. Measurement of hoop strain in this system demonstrates real-world feasibility [24]. Hoop strain refers to the circumferential stress or deformation experienced by a pipeline due to internal pressure. Accurate measurement of hoop strain helps in monitoring the pipeline's structural health and preventing potential failures. Fig. 12 shows the overall schematic configuration of a high-pressure loop natural gas pipeline

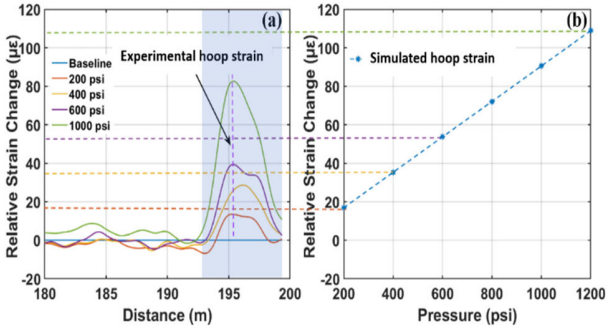

Fig. 11. (a) Experimental results showing relative hoop strain measured for different levels of pipe pressure at ambient room temperature of approximately 22.5 °C (the vertical dotted line was used to calculate the pressure coefficient). (b) Simulated relative strain with respect to pipe pressure variations.

used for testing, which has a 4-in outer diameter steel piping section. The test section and leak locations are highlighted in Fig. 12(a). Using strong adhesive glue, the test pipe section was wound circumferentially with 10 m of standard single-mode fiber (SMF) and DBPF (illustrated in Fig. 12 inset) and coupled to the BOTDA system. The test section wrapped with fiber was covered with a silicon gasket sheet to minimize other environmental factors, such as excessive humidity, or moisture, or uneven heating due to sunlight.

After training the DNN algorithm, the BFSs were directly retrieved from the raw BGS data. Initially, the baseline was measured at ambient temperature with no pressure in the pipe. Brillouin frequencies were swept from 9.8 to 11.05 GHz with a step of 3 MHz. The measured raw data is illustrated in Fig. 13(a). We can see the pressure variations inducing changes in the installed fiber locations around 24.8 km (SMF) and 25.18 km (DBPF) as shown in Fig. 13(b). The BOTDA system was placed in an air-conditioned control room, where the lead-in fiber was connected from the BOTDA system to the sensing fiber installed on the test pipe section. All the measurements were taken from the control room, which is ~10 m away from the test pipe location. It is worthwhile to mention that each measurement time takes more than six minutes to sweep between 9.8 and 11.05 GHz to cover the BGS spectra of both the SMF and DBPF fibers.

After measuring the raw BGS data, we processed it with the proposed PDNN algorithm for rapid, accurate BFS estimation. The relative BFS distribution over the fiber distance is illustrated in Fig. 14. The baseline measurement was taken in the morning around 8 AM at ambient environmental conditions, such as a temperature of ~19.5 °C, while the pipe was not under any pressure. After that, the pipe pressure was increased to 100, 200, 400, 800, and 1000 psi and held for 45 min while measurements were taken. Fig. 14 makes it clear that the ambient temperature increased from 8 AM when the baseline measurement was taken, to 12 PM when the 1000 psi measurement was carried out. Where the SMF fiber had been placed on the test pipe segment, the BFS change was sensitive to both strain and temperature and the BFS distribution experienced both pressure-induced hoop strain and pipe temperature. With conventional SMF fiber, the cross-sensitivity problem cannot be resolved.

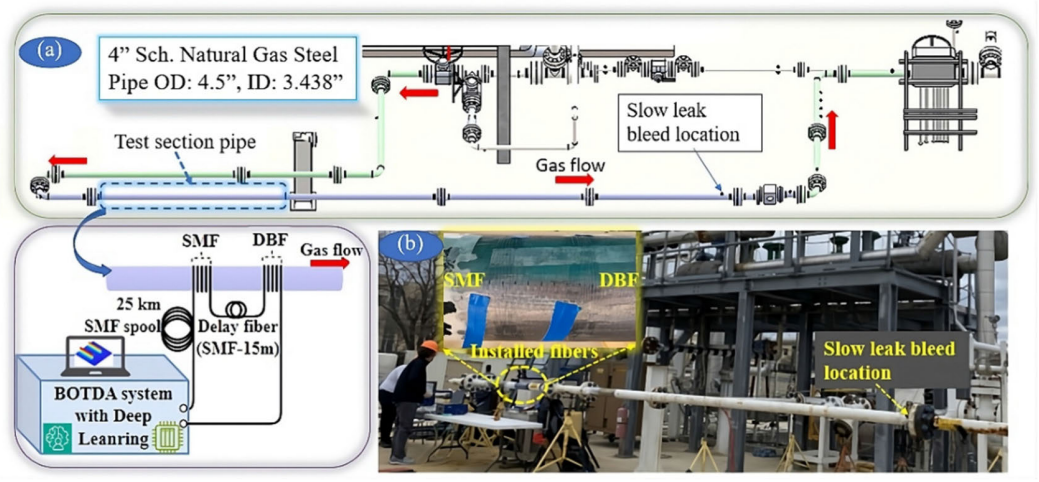

Fig. 12. High-pressure loop natural gas pipeline testing facility with installed fiber optic sensors. (a) Overall schematic illustration. (b) Photograph of the overall test facility with test section pipe.

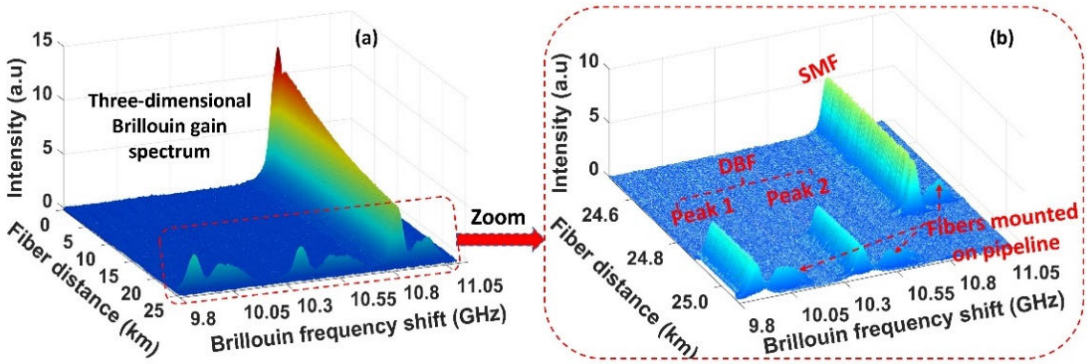

Fig. 13. Measured 3-D BGS spectrum of (a) overall FUT and (b) zoomed-in-view of fiber mounted on test section pipe.

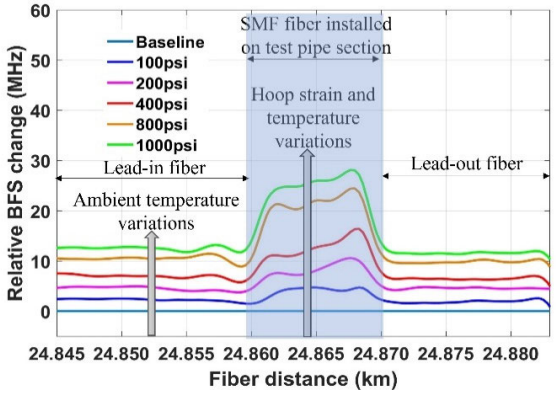

Fig. 14. Relative BFS distribution of conventional SMF at various pipe pressure levels. The influence of temperature fluctuations on the hoop strain measurement is evident and cannot make discriminative temperature and strain measurements.

Using the DPBF, we next showed that accurate pressure estimation is possible through hoop-strain measurement in the field. Based on the calculated strain and temperature coefficients of DBPF, the calibrated hoop strain distribution is illustrated in Fig. 15(a). Only the pipe hoop strain was measured once the temperature changes were successfully removed. At each pressure level, the averaged hoop strain was calculated and shown in Fig. 15(b), where the average hoop strain was calculated from the length of installed sensing fiber highlighted in blue in Fig. 15(a). A pipe hoop strain of approximately 300 $\mu\varepsilon$ was found at an internal pressure of 1000 psi. The test pipe's pressure was then fixed at 1000 psi and several measurements were taken. The measured relative BFS distribution over the fiber distance is shown in Fig. 16 as leaks were simulated in the pipe. A valve that was mounted on the pipe flow loop was opened to simulate the leakage process [shown in Fig. 12(b)]. The leak valve on the pipeline flow loop was opened and the methane leaked out slowly. A negative pressure change wave was created at the leak location by the simulated leak, and it spread throughout the pipeline. It was found that our detection method was sensitive enough to detect pressure changes caused by the simulated leak that was located about 6 m from the installed fiber on the test section.

To measure the leak-induced hoop strain changes, the baseline strain was first measured at 1000 psi. Thereafter, a slow bleed leak was introduced by opening a valve [shown in Fig. 12(b)]. Based on the pressure gauge reading, the valve was kept open until it reached the 900 psi pressure level and then the valve was closed. During this time, few BOTDA measurements were taken. Fig. 16 shows the relative BFS

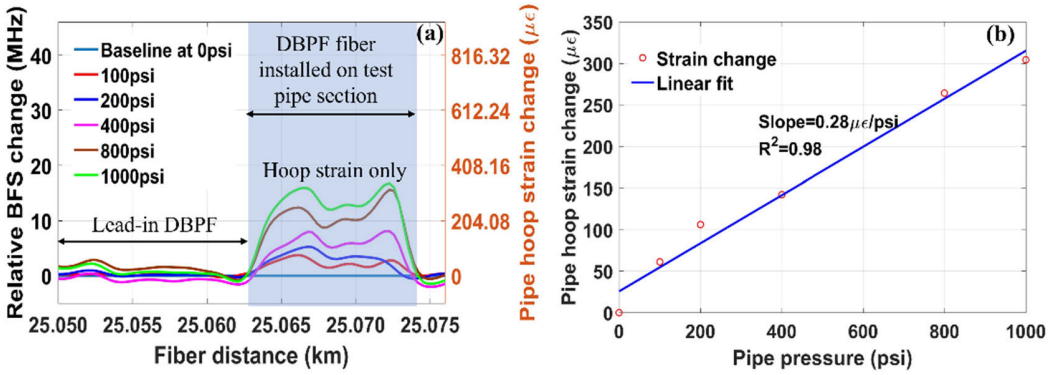

Fig. 15. (a) Calibrated relative BFS distribution and corresponding pipeline hoop strain under various pipe pressures up to 1000 psi. The temperature influence on the hoop strain measurement was calibrated using the multi-peak DBPF sensing fiber. (b) Calculated pipeline hoop strain versus pipe pressure.

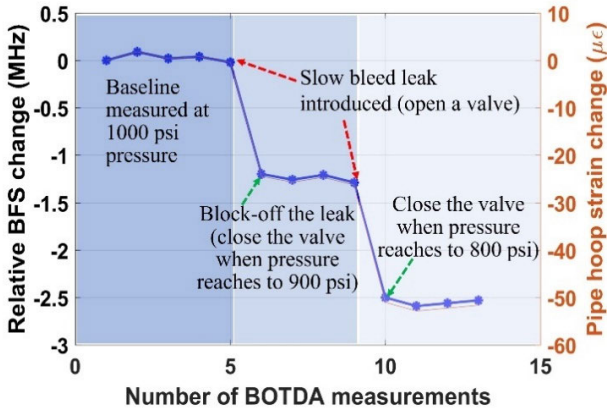

Fig. 16. Relative BFS change and its corresponding pipeline hoop strain alteration during simulated leakage.

changes and corresponding hoop strain changes caused by the leaks. This demonstration shows that any potential leaks can be detected in real-time and catastrophic failure caused by the leak can be prevented [25]. This suggests that the DOFS system can identify natural gas pipeline leaks through changes in leakage-induced hoop strain. It is important to mention that while the proposed leak detection method is based on hoop strain change, this method may also be used for corrosion monitoring, where the hoop strain will change as a result of pipeline corrosion [26].

IV. Conclusion

In conclusion, we developed and demonstrated a robust method for measuring both hoop strain and temperature along a natural gas pipeline. Cross-sensitivity between the strain and temperature was mitigated by using a specialty multi-Brillouin peak fiber. This enabled simultaneous measurement of both parameters using only one optical fiber and interrogator. In addition, considering the low processing speed of conventional curve fitting methods, a novel PDNN algorithm was used to accelerate the BOTDA data processing for rapid BFS estimation with confidence intervals. Additionally, a simulation model was performed to compare the circumferential or hoop strain of the pipe with the experimental hoop strain measured using the BOTDA system. This can enable the estimation of internal pipe pressures using measured hoop strain. Pilot-scale testing was carried out using a natural gas high-pressure loop of 4-in outer diameter steel pipe, and the hoop strain of approximately 300 $\mu\varepsilon$ was observed at an internal pipe pressure of 1000 psi. During the pilot-scale testing, a simulated leak was introduced, and the corresponding hoop strain changes were measured, which suggested accurate leak detection in real-time. These results show that the proposed method is a viable way to monitor pressure and detect leaks along the section of natural gas pipelines.

Acknowledgment

Research performed by Leidos Research Support Team (LRST) staff and subcontract to University of Pittsburgh was conducted under the RSS contract.

References

[1] G. Molnar, "Economics of gas transportation by pipeline and LNG," in *The Palgrave Handbook of International Energy Economics*, M. Hafner and G. Luciani, Eds., Cham, Switzerland: Springer, 2022, pp. 23–57.

[2] S. C. Bhatia, "Advanced renewable energy systems: Biogas," in *Advanced Renewable Energy Systems*, S. C. Bhatia, Ed., Sawston, U.K.: Woodhead Publishing India, 2014, pp. 426–472.

[3] R. E. Emanuel, M. A. Caretta, L. Rivers, and P. Vasudevan, "Natural gas gathering and transmission pipelines and social vulnerability in the United States," *GeoHealth*, vol. 5, no. 6, Jun. 2021, Art. no. e2021GH000442.

[4] J. Yu et al., "Methane emissions from natural gas gathering pipelines in the Permian basin," *Environ. Sci. Technol. Lett.*, vol. 9, no. 11, pp. 969–974, Nov. 2022.

[5] M. Ho, S. El-Borgi, D. Patil, and G. Song, "Inspection and monitoring systems subsea pipelines: A review paper," *Struct. Health Monitor.*, vol. 19, no. 2, pp. 606–645, Mar. 2020.

[6] M. Coramik and Y. Ege, "Discontinuity inspection in pipelines: A comparison review," *Measurement*, vol. 111, pp. 359–373, Dec. 2017.

[7] P. Lu et al., "Distributed optical fiber sensing: Review and perspective," *Appl. Phys. Rev.*, vol. 6, no. 4, Dec. 2019, Art. no. 041302.

[8] I. Ashry et al., "A review of distributed fiber–optic sensing in the oil and gas industry," *J. Lightw. Technol.*, vol. 40, no. 5, pp. 1407–1431, Mar. 1, 2022.

[9] X. Feng, Y. Han, Z. Wang, and H. Liu, "Structural performance monitoring of buried pipelines using distributed fiber optic sensors," *J. Civil Struct. Health Monitor.*, vol. 8, no. 3, pp. 509–516, Jul. 2018.

[10] M. Bertulessi, D. F. Bignami, I. Boschini, M. Longoni, G. Menduni, and J. Morosi, "Experimental investigations of distributed fiber optic sensors for water pipeline monitoring," *Sensors*, vol. 23, no. 13, p. 6205, Jul. 2023.

[11] S. Zhang, B. Liu, and J. He, "Pipeline deformation monitoring using distributed fiber optical sensor," *Measurement*, vol. 133, pp. 208–213, Feb. 2019.

[12] M. A. Soto and L. Thévenaz, "Modeling and evaluating the performance of Brillouin distributed optical fiber sensors," *Opt. Exp.*, vol. 21, no. 25, pp. 31347–31366, 2013.
[13] A. Venketeswaran et al., "Recent advances in machine learning for fiber optic sensor applications," *Adv. Intell. Syst.*, vol. 4, no. 1, Jan. 2022, Art. no. 2100067.
[14] D. Qi, J. Li, X. Guan, and C.-K. Chan, "Dynamic polarization-insensitive BOTDA in direct-detection OFDM with CNN-based BFS extraction," *Opt. Exp.*, vol. 30, no. 5, p. 7725, 2022.
[15] B. Wang, L. Wang, N. Guo, Z. Zhao, C. Yu, and C. Lu, "Deep neural networks assisted BOTDA for simultaneous temperature and strain measurement with enhanced accuracy," *Opt. Exp.*, vol. 27, no. 3, p. 2530, 2019.
[16] H. Zheng, Y. Yan, Y. Wang, X. Shen, and C. Lu, "Deep learning enhanced long-range fast BOTDA for vibration measurement," *J. Lightw. Technol.*, vol. 40, no. 1, pp. 262–268, Jan. 1, 2022.
[17] B. Wang, N. Guo, L. Wang, C. Yu, and C. Lu, "Denoising and robust temperature extraction for BOTDA systems based on denoising autoencoder and DNN," in *Proc. 26th Int. Conf. Opt. Fiber Sensors*, Lausanne, Switzerland, 2018, p. WF29.
[18] N. Lalam et al., "Pilot-scale testing of natural gas pipeline monitoring based on phase-OTDR and enhanced scatter optical fiber cable," *Sci. Rep.*, vol. 13, no. 1, p. 14037, Aug. 2023.
[19] N. Lalam et al., "Multi-parameter distributed fiber optic sensing using double-Brillouin peak fiber in Brillouin optical time domain analysis," *Opt. Exp.*, vol. 31, no. 22, p. 36590, 2023.
[20] A. Venketeswaran, N. Lalam, P. Lu, S. R. Bukka, M. P. Buric, and R. Wright, "Robust vector BOTDA signal processing with probabilistic machine learning," *Sensors*, vol. 23, no. 13, p. 6064, Jun. 2023.
[21] N. Lalam, A. Venketeswaran, P. Lu, and M. Buric, "Probabilistic deep neural network based signal processing for Brillouin gain and phase spectrums of vector BOTDA system," *Proc. SPIE*, vol. 11692, Mar. 2021, Art. no. 1169213.
[22] Z. Jia, S.-C. Ho, Y. Li, B. Kong, and Q. Hou, "Multipoint hoop strain measurement based pipeline leakage localization with an optimized support vector regression approach," *J. Loss Prevention Process Industries*, vol. 62, Nov. 2019, Art. no. 103926.
[23] V. Vullo, "Circular cylinders and pressure vessels," in *Springer Series in Solid and Structural Mechanics*. Cham, Switzerland: Springer, 2014, p. 388.
[24] V. Chmelko, M. Garan, and M. Šulko, "Strain measurement on pipelines for long-term monitoring of structural integrity," *Measurement*, vol. 163, Oct. 2020, Art. no. 107863.
[25] F. Idachaba and O. Tomomewo, "Surface pipeline leak detection using realtime sensor data analysis," *J. Pipeline Sci. Eng.*, vol. 3, no. 2, Jun. 2023, Art. no. 100108.
[26] L. Ren, T. Jiang, D.-S. Li, P. Zhang, H.-N. Li, and G.-B. Song, "A method of pipeline corrosion detection based on hoop-strain monitoring technology," *Struct. Control Health Monitor.*, vol. 24, no. 6, p. e1931, Jun. 2017.

Nageswara Lalam (Member, IEEE) is currently a Senior Research Scientist with the U.S. Department of Energy's National Energy Technology Laboratory (NETL), Pittsburgh, PA, USA. He has authored or co-authored more than 70 technical publications and holds six U.S. patents including under review. His research interests include distributed fiber optic sensors, nonlinear fiber optics, optical communications, optoelectronics, fiber interferometers, quantum fiber sensors, AI/ML for sensor data analytics, and digital signal processing.

Dr. Lalam was a Technical Program Committee Member of the International Conference on Optical Fiber Sensors (OFS). He has received the R&D 100 Awards for the "Transformer Watchman" monitoring system in 2023 and for the "Ultrasonic Photonics" pipeline non-destructive evaluation system in 2024. He is an Associate Editor of IEEE SENSORS JOURNAL and an Academic Editor of *Journal of Sensors* (Wiley).

Hari Bhatta is currently a Research Scientist with the National Energy Technology Laboratory (NETL), Pittsburgh, PA, USA. His research interests include development of the efficient distributed fiber sensor systems based on the Brillouin and Rayleigh scatterings, to be used for the structural health monitoring of natural gas pipelines infrastructures, digital signal processing, machine learning based data processing, and nonlinear fiber optics.

Sandeep Reddy Bukka received the Ph.D. degree in computational fluid dynamics from the National University of Singapore, Singapore, in 2020.

He is currently a Computational Scientist employed by the Leidos as a NETL Support Contractor with the U.S. Department of Energy National Energy Technology Laboratory, Pittsburgh, PA, USA.

His current research interests include the development of AI-enhanced sensor technologies, pipeline digital twin, simulation models for gas flow through pipelines, and hybrid techniques for sensor fusion and analytics.

Pengdi Zhang is currently pursuing the Ph.D. degree with the Department of Mechanical Engineering and Materials Science, University of Pittsburgh, Pittsburgh, PA, USA.

He is a Mechanical Engineer with the Department of Mechanical Engineering and Materials Science, University of Pittsburgh. His work focuses on developing advanced simulation tools for guided wave propagation and pipeline health monitoring using reduced order models (Rom), and machine learning techniques. His expertise also includes integrating acoustic signal analysis with physics-based AI to enhance structural health monitoring and non-destructive evaluation.

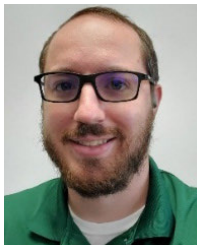

Nathan Diemler received the M.S. degree in inorganic/materials chemistry from the University of Pittsburgh, Pittsburgh, PA, USA, in 2019.

He is currently a Research Project Manager (formerly Materials Scientist) employed by the Leidos as a NETL Support Contractor with the U.S. Department of Energy's National Energy Technology Laboratory, Pittsburgh. He supports projects related to energy infrastructure, methane and hydrogen technologies, and flare gas conversion.

Alexander Shumski received the Ph.D. degree in inorganic/materials chemistry from Purdue University, West Lafayette, IN, USA, in 2021.

He is currently a Materials Scientist employed by the Leidos as an NETL Support Contractor with the U.S. Department of Energy National Energy Technology Laboratory, Pittsburgh, PA, USA. His current areas of research focus are the development of optical sensor materials, pH sensors, and sensors for post-combustion carbon capture solvent degradation.

Paul R. Ohodnicki (Member, IEEE) received the B.Phil. degree in engineering physics from the University of Pittsburgh, Pittsburgh, PA, USA, in 2005, the B.A. degree in economics from the University of Pittsburgh, in 2005, and the M.S. and Ph.D. degrees in materials science and engineering from Carnegie Mellon University, Pittsburgh, in 2006 and 2008, respectively.

He is currently a RK Mellon Faculty Fellow in energy with the Department of Mechanical Engineering and Materials Science, University of Pittsburgh, with a secondary appointment in electrical and computer engineering. In addition, he is the Engineering Science Program Director and the Founding Director of the Advanced Magnetics for Power and Energy Development Consortium, Pittsburgh. He is the Chief Technology Officer and the Co-Founder of CorePower Magnetics, Pittsburgh. Prior to his current roles, he was a Materials Scientist and the Technical Portfolio Lead of the Functional Materials Team, Materials Engineering and Manufacturing Directorate, National Energy Technology Laboratory. He has authored or co-authored more than 200 technical publications and holds more than 30 patents, with more than 30 additional patents under review.

Dr. Ohodnicki was a recipient of numerous awards and recognitions, including the R&D 100 Award in 2019 and 2022, the Federal Employee Rookie of the Year Award in 2012, the Presidential Early Career Award in science and engineering in 2016, and the Advanced Manufacturing and Materials Innovation Category Award for the Carnegie Science Center in 2012, 2017, and 2019. In 2017, he was a nominee for the Samuel J. Heyman service to America Medal.

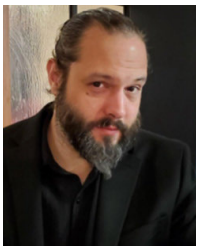

Michael P. Buric is currently a Research Scientist with the Functional Materials Development Team, Lab's Research and Innovation Center, National Energy Technology Laboratory (NETL), Morgantown, WV, USA. He is also the Lead Laser Safety Officer of NETL in addition to overseeing several energy-related research projects. His current research interests include the modeling and fabrication of fiber-based optical sensors and devices, harsh-environment sensing for energy applications, laser-heated pedestal growth of single-crystal optical fibers, novel waveguide fabrication, distributed sensing, fiber embedding, additive manufacturing, and applications of Raman spectroscopy.

Dr. Buric was awarded several patents and is published extensively in the proceedings of SPIE and elsewhere. He was a recipient of the SPIE's 2017 Rising Researcher Award and the 2020 Carnegie Science Center Innovation Award in energy. He received the R&D 100 Awards, including the "NuSense" technology in 2022, the "Transformer Watchman" monitoring system in 2023, and the "Ultrasonic Photonics" pipeline NDE system with various teams in 2024.

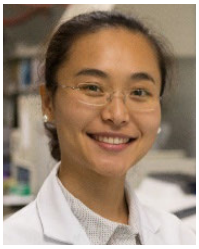

Ruishu F. Wright received the B.S. degree in metallurgical science and engineering from the Central South University, Changsha, China, in 2009, the M.S. degree in chemical engineering and technology from Tsinghua University, Beijing, China, in 2012, and the Ph.D. degree in energy and mineral engineering and electrochemical science and engineering from The Pennsylvania State University, University Park, PA, USA, in 2016.

She is currently a Research Physical Scientist with the U.S. Department of Energy, National Energy Technology Laboratory. She is the Technical Portfolio Lead of Methane Mitigation Technologies and a Principal Investigator of multiple projects and coordinates research and develpoment efforts of an interdisciplinary team to develop real-time sensors (e.g., otpical fiber sensors and wireless sensors) and functional sensitive materials. She has published more than 50 technical articles, given more than 40 presentations at conferences, and holds ten pending. Her research interests include structural health monitoring and gas leak detection of natural gas and hydrogen pipelines, supporting safe hydrogen transportation and subsurface hydrogen storage, wellbore integrity monitoring of carbon storage wells, and power grid monitoring.

Dr. Wright was awarded the U.S. patents on sensor technologies and the two R&D 100 Awards in 2023 and 2024.